Pathogenic variants in *TNNC2* cause congenital myopathy due to an impaired force response to calcium

ONLINE SUPPLEMENT

Martijn van de Locht[1], Sandra Donkervoort[2], Josine M. de Winter[1], Stefan Conijn[1], Leon Begthel[1], Benno Kusters[3], Payam Mohassel[2], Ying Hu[2], Livija Medne[4], Colin Quinn[5], Steven A. Moore[6], A. Reghan Foley[2], Gwimoon Seo[7], Darren T. Hwee[8], Fady I. Malik[8], Thomas Irving[9], Weikang Ma[9], Henk Granzier[10], Erik-Jan Kamsteeg[3], Kalyan Immadisetty[11], Peter Kekenes-Huskey[11], José R. Pinto[12], Nicol Voermans[3], Carsten G. Bönnemann[2 #], Coen A.C. Ottenheijm[1,10 #]

[1]Dept of Physiology, Amsterdam UMC, Amsterdam, The Netherlands; [2]Neuromuscular and Neurogenetic Disorders of Childhood Section, National Institute of Neurological Disorders and Stroke, National Institutes of Health, Bethesda, MD, USA; [3]Dept. of Neurology and Human Genetics, Radboud University Medical Center, Nijmegen, Netherlands; [4]Division of Human Genetics, Dept of Pediatrics, Individualized Medical Genetics Center, Children's Hospital of Philadelphia, Philadelphia, PA, USA; [5]Dept of Neurology, University of Pennsylvania, Philadelphia, PA, USA; [6]Dept of Pathology, University of Iowa Carver College of Medicine, Iowa City, IA, USA; [7]Protein Expression Facility, Institute of Molecular Biophysics, Florida State University, Tallahassee, FL, USA; [8]Research and Early Development, Cytokinetics Inc., South San Francisco, CA, USA; [9]BioCAT, Illinois Institute of Technology, Chicago, IL, USA; [10]Dept of Cellular and Molecular Medicine, University of Arizona, Tucson, AZ, USA; [11]Dept of Cell and Molecular Physiology, Loyola University, Chicago, IL, USA; [12]Dept of Biomedical Sciences, The Florida State University College of Medicine, Tallahassee, FL, USA.

[#] Both authors contributed equally.

CORRESPONDING AUTHOR: Coen A.C. Ottenheijm, O|2 Labgebouw, De Boelelaan 1108, 1081 HZ, Amsterdam, +31 (0)20 4448123, c.ottenheijm@amsterdamumc.nl

DISCLOSURE. We have no competing interest to disclose.

KEYWORDS. Troponin C, Sarcomere, Troponin activator, Congenital myopathy.

SUPPLEMENTAL METHODS

Patient Recruitment and Sample Collection

Two unrelated Caucasian families, one from the United States and one from the Netherlands were included in the study. Medical history was obtained, clinical evaluation and muscle biopsies were performed as part of the standard neurologic evaluation. DNA was extracted from blood and saliva based on standard procedures. Muscle biopsies were obtained from spinal accessory muscle (family 1, patient 1; F1:P1) during scoliosis surgery and quadriceps muscle (control subjects and family 2, patient 1; F2:P1) using a Bergström muscle biopsy needle while the patient's skin was locally anesthetized. F1:P1 was biopsied at age 26 years, F2:P1 was biopsied at age 19 years, and control subjects were biopsied at age 44-65 years. The biopsies were snap frozen in liquid nitrogen immediately after excision and stored at -80 °C until used. For patients' and control subjects' general information, see Table 2. A detailed clinical description of both patients' families is in Table 1.

Immunohistochemistry

For F1:P1, NADH staining was used to quantify the cross-sectional area (CSA) of the slow twitch and fast twitch myofibers. For control subjects and F2:P1 a mATPase 4.2 staining was used to quantify the CSA. To analyze the cross-sections, open source Fiji software was used to manually trace the circumference of the myofibers and calculate the Feret diameter (1).

Low-angle X-ray diffraction

Low-angle X-ray diffraction experiments were performed on the Biophysics Collaborative Access Team beamline 18ID at the Advanced Photon Source, Argonne National Laboratory, Argonne, IL (2).

From patient F1:P1, twenty-eight fibers were mounted and aligned in one plane between two-halves of an electron microscopy grid. These preparations were mounted on a custom X-ray diffraction/muscle mechanics setup designed to fit into the X-ray diffraction instrument. The preparations were attached to a force transducer element (ASI 403A, Aurora Scientific) at one end and to a fixed hook at the other end. Sarcomere length was determined using the first-order diffraction band from an He-Ne laser. Sarcomere length was set at 2.5 μm. The small-angle diffraction camera length was ~3m, and X-ray energy was 12keV. The X-ray total exposure times were 1 second with an incident flux of $\sim 1 \times 10^{12}$ photons/s, and the X-ray diffraction patterns were collected with the use of a Pilatus 3 1M pixel array detector (Dectris, Baden-Dättwil, Switzerland). Images were taken in 100 frame bursts of 10 millisecond frames separated by 90 milliseconds with the shutter closed to reduce radiation damage. In addition, the samples were translated in the beam during the exposures to further reduce radiation damage. The axial spacing of the Tn3 reflection at 12.7 nm and the 6^{th} actin layer line at 5.9 nm was measured as described previously (3).

Molecular dynamics simulations

Human *TNNC2* with Ca^{2+} bound (holo) was modeled based on the Oryctolagus cuniculus holo (bound with four Ca^{2+} ions; two in each domain) troponin C (*Tnnc2*) X-ray crystal structure (PDB: 2TN4) (4). Human *TNNC2* shares 99% sequence identity with the Oryctolagus cuniculus sequence; in the human sequence, there is a substitution of proline at position 112 vs. alanine (5). Accordingly, we introduced the A112P substitution and the addition of four residues (156-160) missing from the 2TN4 structure via the CHARMM-GUI web server (6). In addition, we reverted the C99L mutation introduced by the crystallographers back to cysteine using

CHARMM-GUI to match the original sequence. All four Ca^{2+} that are in the X-ray structure were retained. For modeling the human *TNNC2* Ca^{2+}-free state (apo), we again used an Oryctolagus cuniculus apo X-ray crystal structure (PDB: 1A2X) that was crystallized with a segment of C-terminal troponin I (TnI) (7). The 1A2X structure reflects two Ca^{2+} bound to the C-domain, while the N-domain is free of bound Ca^{2+} ions. As with the holo state, A112P was substituted via CHARMM-GUI and we introduced a missing threonine residue at position 1. The C-terminal TnI segment in the apo X-ray structure was removed as it does not directly interact with the N-terminal domain of TnC.

The CHARMM-GUI web server was also used to build the solvated KCl-containing human *TNNC2* simulation systems. In total six systems were built, three apo (Apo:WT, Apo:D34Y, and Apo:M79I) and three holo (Holo:WT, Holo:D34Y, Holo:M79I). Each system was placed in a rectangular TIP3P water box and KCl was added to neutralize the system and raise the ionic strength to 0.15M (8). The box size in each apo system is 89 *X* 89 *X* 89 $Å^3$ and contains one *TNNC2* protein, 85 potassium and 60 chloride ions, 21,096 waters, two Ca^{2+} ions (65,862 total atoms). Each holo system box size is 99 *X* 99 *X* 99 $Å^3$, and contains one *TNNC2* protein, 105 potassium and 84 chloride ions, 29,450 waters, four Ca^{2+} ions (90,970 total atoms). Each system was simulated via all atom MD using the Amber 18 MD simulation engine and the input files for conducting MD simulations were generated using CHARMM-GUI input generator (9, 10). The CHARMM36 all-atom additive force field parameters were used to parameterize all components of the system (11). Each system was minimized for 50,000 steps, of which the first 2500 steps used the steepest-descent algorithm and the remaining using the conjugate gradient algorithm while applying positional restraints to the protein with a force constant of 1 kcal/mol/$Å^2$. Each system was then equilibrated for 5 ns with a time step of 1 fs in the NVT ensemble while still having the weak restraints (K = 1 kcal/mol/$Å^2$) imposed on the protein (12). For the production runs, each system was simulated in triplicate with each comprising approximately 1μs simulation data under periodic boundary conditions using the NPT ensemble with a constant temperature of 300K and 1 atm constant pressure. The Langevin

integrator and Berendsen barostat were used for this ensemble (12–14). The SHAKE algorithm was used to restrain bonds associated with hydrogens (15). A nonbonded cutoff 10 Å and the Particle Mesh Ewald (PME) method was used to treat long-ranged electrostatic interactions (16, 17). Overall, we collected approximately 18μs of simulation data (6 systems *X* 3 trials *X* 1μs = 18μs) using a 2 fs time step. Data were saved for every 0.1 ns and a total of 5000 data points from each MD trial were used for each system for analysis, yielded 15,000 data points total for the three replicas. For MD simulations with the intact troponin complex comprising TnC, TnI and TnT, we used the crystal structure of cardiac TnC (PDB: 1J1E) (18). The missing residues were modeled using the Rosetta software (19). The systems for the MD simulation (WT and M79I) were built using CHARMM-GUI. The size of each system is 160 X 160 X 160 $Å^3$. The total number of atoms in each system were 345,255. Three trials of each system were simulated, each trial for 200 ns (600 ns for each system). Force field parameters and the MD procedure adopted were similar to what was explained earlier for other systems. Simulations were conducted on a local GPU cluster as well as on XSEDE resources. VMD tcl plugins as well as cpptraj (part of the Amber package) were used for data analysis (20). ProDy software package was used for PCA analysis. All code written in support of this publication are publicly available at https://bitbucket.org/pkhlab/pkh-lab-analyses. Input files for simulations as well as routines for analyses are distributed as open-access materials at https://github.com/huskeypm/pkh-lab-analyses.

Myofiber contractility experiments

We adapted previously described methods to investigate the contractile properties of myofibers of patients (F1:P1, n = 19 fibers; F2:P1, n = 22 fibers) and healthy controls (N = 6, n = 78 fibers) (21–24). In brief, small sections (2×2 mm) were isolated from the biopsies and glycerinated for 24 h at -20°C. Single myofibers from control subjects (average age at biopsy: 47±8 years), F1:P1 and F2:P2 were dissected from the muscle strips and clipped between aluminum foil T-clips. Myofibers were permeabilized in 1% (v/v) Triton^{TM} X100/relaxing

solution, then mounted between a length motor (ASI 315C I; Aurora Scientific, Aurora, ON, Canada) and a force transducer element (ASI 403A, Aurora Scientific) in a permeabilized myofiber apparatus (ASI 802D, Aurora Scientific) mounted on top of an inverted microscope (Axio Observer A1; Zeiss, Oberkochen, Germany). Sarcomere length was set to 2.5 μm using a using a 40x objective, high-speed VSL camera and ASI 900B software (Aurora Scientific). Myofiber length, width, and depth were measured at three points along the myofiber using a 10x objective, a prism, and a custom-made mirror mounted in the bath. CSA was calculated with the average width and depth of the myofiber assuming an elliptical cross-section. In vivo, skeletal muscle typically is activated at submaximal calcium levels producing force between 10-65% of maximal force (25, 26). Therefore, we determined the force response of myofibers to incremental Ca^{2+}-concentrations. (Note that exposure to incremental Ca^{2+}-concentrations renders similar force-pCa relations as exposure to randomly ordered Ca^{2+}-concentrations (27).) The steady-state forces measured at each Ca^{2+}-concentration were normalized to the maximal force (obtained at pCa 4.5). The resulting curve was fitted to the Hill equation ($Y = 1 / [1+10^{nH (pCa - pCa_{50})}]$) (28, 29). During the permeabilized myofiber contractility the temperature was kept at 20°C using a temperature controller (ASI 825A, Aurora Scientific).

The criteria of acceptance for further analysis included: (1) preserved striation pattern (also required to set sarcomere length); (2) the force at the final pCa 4.5 had to be higher than 90% of the force during the first activation at pCa 4.5. Note that each myofiber underwent two maximal activations (pCa 4.5) and five submaximal activations (pCa 7.0 – 6.0 – 5.8 – 5.6 – 5.4); (3) preserved sarcomere length in the myofibers after completion of the experimental protocol (to assure that the myofiber was well set in the clip). Applying these criteria, ~70% of the myofiber experiments were included in the results shown.

Protein Expression and purification of fsTnC

An expression vector encoding human *TNNC2* was synthesized by Eurofins genomics, and inserted between the NdeI and BamHI sites of pet11b, using Gibson Assembly (New England

Biolabs). Correct insertion was verified with Sanger sequencing of the construct. The fast skeletal Troponin C wild type and mutants (D34Y and M79I) were transformed into *E.coli* BL21-CodonPlus (DE3)-RIPL on the LB plate with ampicillin (50 µg/ml) and chloramphenicol (34 µg/ml). The selected colony was picked, transferred to 30 ml of LB and placed overnight in a shaking incubator at 37 °C at 200 rpm. Next morning, 14 ml of culture was inoculated to 2.8L Fernbach flask containing 2 L of LB with ampicillin and chloramphenicol. The cells were grown at 37 °C at 200 rpm until absorbance reached 0.8 at A600 nm. Then temperature was changed from 37 °C to 15°C and all cultures were induced with 0.5 mM Isopropyl β-D-1-thiogalactopyranoside (IPTG) followed by additional overnight growth at 15 °C. Bacterial cells were harvested for 30 min at 4,000 rpm. Cell pellets were resuspended in 30 ml of lysis buffer (50 mM Tris-Cl pH 7.8, 6M Urea, 1 mM EDTA, and 1 mM fresh Dithiothreitol (DTT) and lysed on ice using a Branson Sonifier set at 30% amplitude (cycles of 1 sec on and 1 sec off) for 1 min. After, disrupted cell pellets were clarified by centrifugation at 15,000 rpm for 30 min and the supernatant was collected. The HiTrap Q HP column was equilibrated with lysis buffer and the supernatant was loaded onto it. After loading the supernatant, the column was washed with 200 ml of lysis buffer. Elution was performed with a linear gradient of 100 ml from 0 to 0.6 M KCl. Each fraction of peaks was confirmed by 4-20% SDS-PAGE gradient gels and the cleanest fractions were pooled. These fractions were subsequently concentrated and loaded onto a Hiload 16/600 Superdex 200 pg column with Gel filtration buffer (50 mM Tris-Cl pH 7.5, 50 mM NaCl, 1 mM MgCl2, 1 mM CaCl2, and 1 mM DTT). Eluted fractions were confirmed by 4-20% SDS-PAGE gradient gels. The cleanest fractions were pooled and dialyzed against 5 mM Ammonium Bicarbonate. After dialysis, the protein was lyophilized and stored at -80 °C.

Extraction and reconstitution of fsTnC in single permeabilized myofibers

Single myofibers were isolated and permeabilized as described above. We adapted previous methods to reconstitute fsTnC (30). Endogenous fsTnC was extracted from fast twitch myofibers by incubation on a shaker for 2 hours at room temperature in a rigor solution (5mM

EDTA and 20mM Tris at pH 7.2) containing protease inhibitors (1mM E-64, 1mM Leupeptin, 1mM DTT and 1,25mM). Maximal force was determined before and after fsTnC extraction by exposing the fibers to a pCa 4.5 solution at a sarcomere length of 2.5µm. From this we determined the force drop after extraction compared to baseline force before extraction. Subsequently, the fibers were reconstituted with recombinant fsTnC by incubating the myofibers on a shaker for 2 hours at room temperature in a fsTnC-suspension in relaxing solution (~1 mg/mL TnC) containing protease inhibitors (1mM E-64, 1mM Leupeptin, 1mM DTT and 1,25mM PMSF). In these experiments recombinant WT-, D34Y-fsTnC, and M79I-fsTnC was used for control myofibers and WT-fsTnC for F1:P1 and F2:P1 myofibers. Hereafter, the maximal force and force-[Ca^{2+}] relationships were determined. After completion of the protocol the myofibers were saved in sample buffer for protein analysis. Sham reconstitution experiments were performed, to rule out the effect of the experiment duration and procedure on contractile parameters of the myofibers. Multiple conditions were tested: (1) Myofibers of which fsTnC was extracted were exposed to 25% reconstitution buffer in relaxing solution containing protease inhibitors (1mM E-64, 1mM Leupeptin, 1mM DTT and 1,25mM PMSF) to determine possible detrimental effects of the buffer used; (2) To rule out run-down of force due to the length of the protocol, a similar protocol was performed, but the extraction solution and protein suspension were replaced with relaxing solution containing protease inhibitors. Note that neither the 25% reconstitution buffer nor the length of the protocol affected myofiber contractility.

Effect of *tirasemtiv* on myofiber contractility

We tested the ability of *tirasemtiv*, a fast skeletal muscle troponin activator, to augment the contractile force of fast twitch patients' myofibers. Single myofibers were isolated and permeabilized as described above. The protocol was adapted from previous work and the concentration-response curve was determined previously (31). For each myofiber the force-pCa relation was determined as described above: (1) in the presence of 1% dimethylsulfoxide

(DMSO) and (2) in the presence of 10 µM *tirasemtiv*. Note that 1% DMSO did not affect myofiber contractility. The order of the protocol was alternated between fibers. Note that we also tested the effect of *tirasemtiv* on slow twitch myofibers: $[Ca]_{50,F1:P1}$ = 1.84±0.09 in DMSO and 1.63±0.12 in *tirasemtiv*; $[Ca]_{50,F2:P1}$ = 2.07±0.09 in DMSO and 1.85±0.11 in *tirasemtiv*.

Myosin heavy chain isoform composition of permeabilized myofibers

Determination of the myosin heavy chain isoform composition of the single myofibers used in the contractility assays was performed as described previously (22, 32). First, the fibers were placed in sodium dodecyl sulfate (SDS) sample buffer and were denatured by boiling at 80°C for 2 minutes and electrophoresis was performed for 24 hours at 15°C, a constant voltage of 275V, using a stacking gel containing a 4% acrylamide concentration (pH 6.7), and a separating gel containing 7% acrylamide (pH 8.7) with 30% glycerol (vol/vol). Finally, the gels were stained with SYPRO Ruby protein gel stain and scanned.

SUPPLEMENTAL RESULTS

Clinical presentation

Family 1: Patient 1 (F1:P1; pedigree in Fig.2A) is a 26-year-old male with a history of congenital weakness, vocal cord paralysis, respiratory insufficiency, ptosis and ophthalmoplegia. First concerns arose prenatally with maternal polyhydramnios treated with serial amniocenteses. Fetal movements were reported as normal. He was born full-term by Cesarean section after induction of labor due to fetal distress. At delivery he was noted to have stridor (due to vocal cord paralysis) and respiratory insufficiency and was promptly intubated and a tracheostomy tube was placed by 4 days of age. There was no report of hip dysplasia or torticollis; however, he was noted to be hypotonic (Fig.2B) and to have camptodactyly with contractures bilaterally and a small right ear canal. In addition, ptosis and ophthalmoplegia were noted from an early age. Due to concerns for gastroesophageal reflux and aspiration, a Nissen fundoplication procedure was performed, and a percutaneous endoscopic gastrostomy (PEG) tube was placed. Tube feedings continued until 16 years of age. The respiratory symptoms improved, and he was successfully decannulated by 4 years of age. Gross motor development was delayed. He rolled over by 10 months and walked independently by 17 months. As a toddler, he had difficulties keeping up with his peers. Overall, his strength continued to improve. On examination at age 26 years, P1 had asymmetric right-greater-than-left-sided ptosis. Extraocular movements were notable for bilateral abduction and supraduction limitation. He had mild upper and lower facial weakness. Muscle bulk was reduced globally and he had contractures of the jaw and ankles. Strength testing revealed axial, proximal and distal weakness manifesting as neck flexion 4-/5; deltoid 4+/5; elbow flexion 4+/5 (right), 4/5 (left); elbow extension 4/5 (right), 4-/5 (left); hip flexion 4-/5; hip abduction 4/5; hip adduction 4+/5; ankle plantarflexion 4+/5 (right), 5/5 (left); ankle inversion 4+/5 (right), 5/5 (left); ankle eversion 4/5 (right), 5/5 (left) (MRC-grade). He had a waddling gait, was able to jump and walk on his heels and toes but was unable to get up from a squatting position. Sensation was normal. Reflexes were normal but absent in the ankles.

As a school-age child, he was diagnosed with a learning disability, but graduated from high school. He was diagnosed with osteopenia at age 5 years but has not had a follow-up evaluation since that time. He has a long-standing history of poor appetite and difficulty gaining weight. He developed progressive scoliosis and underwent spinal fusion surgery with rod placement at age 16 years. Electromyography (EMG) and nerve conduction responses were consistent with a chronic myopathic process. Echocardiogram was normal. Pulmonary function testing revealed a reduced forced vital capacity (FVC) of 45% predicted. Muscle MRI showed mild focal fatty infiltration of a few muscles (e.g. paraspinals) with proximal greater than distal involvement of the lower extremity muscles (Fig.2B); brain MRI was normal. Family history was significant for a brother, mother and maternal grandmother presenting with a similar clinical phenotype. His brother declined evaluation by our team. Extensive genetic testing including neuromuscular and ophthalmoplegia next-generation-based sequencing panels were negative.

Family 1: Patient 2 (F1:P2) is the 55-year-old mother of F1:P1. She presented similarly in the immediate neonatal period with early respiratory failure due to stridor and vocal cord paralysis, requiring intubation and tracheostomy. She was noted to have scoliosis by 8 days of age. Her early development was significant for mild delays in motor milestones. She sat unsupported by 8 months of age, rolled over by 1 year of age, was able to walk with a walker by 15 months. She was never able to run, and had difficulties keeping up with her peers. From an early age she noted progressive ptosis for which she underwent eyelid retraction surgery. She reported mild learning disability but also graduated high school. Over the years, she remained relatively stable but there was a gradual worsening of her overall strength. She fatigues when walking long distances or standing for a prolonged period of time. She also reports significant, generalized pain which is exacerbated with normal levels of physical activity and with cold weather. She also has a history of osteopenia, which was first noted at age 45 years. On examination at age 55 years she was found to have mild right ptosis. Extraocular movements were notable for bilateral abduction deficit and mild supraduction limitation. Strength testing

revealed weakness in the 4-/5 range (MRC-grade) affecting neck flexion 4-/5; deltoid 4+/5; elbow flexion 4+/5; elbow extension 4/5; finger extension 4/5; hip flexion 4-/5; hip abduction 4+/5; hip adduction 4-/5; knee flexion 4/5; knee extension 4+/5 and toe extension 4+/5. She has mild upper and lower facial weakness. She has mild scoliosis and a waddling gait. She has contractures of the jaw. Sensation and reflexes were normal. Pulmonary function testing revealed a reduced (FVC) of 73% predicted, with an 11% decline from sitting to supine. Echocardiogram was normal. Muscle MRI showed a similar pattern of muscle involvement as P1, with slightly less involved paraspinal muscles.

Family 1: Patient 3 (F1:P3) is the 76-year-old maternal grandmother of P1. Pregnancy was complicated by breech presentation. At birth, she was noted to have difficulty breathing and stridor, however did not require a tracheostomy. She was never athletic and could not run but was able to function without limitations. She walked by 15 months of age. She was able to climb stairs and jump by 6 years of age. She was subsequently noted to have scoliosis and underwent scoliosis surgery with bone fusion. She remained active without major limitations until age 60 years when she had a compression fracture in her lumbar spine. Since that time, she noticed a gradual worsening in her level of motor function and increased fatigability. At age 74 years she had recurrent pneumonias and was diagnosed with a tracheoesophageal fistula. She has significant osteopenia and a history of six bone fractures including legs, ribs, elbow, and lumbar spine. Examination at age 76 years revealed a high arched palate and facial weakness. She did not have any ptosis. Extraocular movements were notable for subtle abduction limitation and significant limitation in supraduction. Strength was generally mildly reduced with knee flexion 4/5 and knee extension 4-/5 (MRC grade). Reflexes were normal. Gait examination showed a kyphotic posture with an antalgic quality. Pulmonary function testing revealed a reduced FVC of 47% predicted. Echocardiogram showed moderate tricuspid regurgitation and trivial pericardial effusion. Muscle MRI showed mild, focal fatty infiltration of different muscles in a patchy and heterogeneous pattern, with significant involvement of the paraspinal muscles.

Family 2: Patient 1 (F2:P1; Fig.2D; pedigree in Fig.2C) is a now 22-year old female patient, who was born after a pregnancy complicated by polyhydramnios (treated with serial amniocenteses) at term. An intrauterine ultrasound had shown swallowing difficulties. APGAR scores were low (2 and 3 at 5 and 10 minutes) and she was noted to be hypotonic. Because of postnatal swallowing difficulties, she was admitted at the neonatal ICU and nasogastric tube feeding was started. A percutaneous gastrostomy was placed at the age of four months. She had recurrent respiratory tract and urinary tract infections up to three years of age. Motor development was within normal range (standing at 12 months, walking around 18 months); however, she fell frequently resulting in teeth injuries, clavicula fracture at the age of four and a concussion at the age of six. The jaw development was abnormal for which she was referred to a dental surgeon. In childhood, she had difficulties with running leading to limited sports participating. She learned to cycle and ski. At the age of eight, physical examination showed a length of 129 cm (- 1 SD), and a weight of 20 kg (- 2 SD). Eye movements were normal, she had a pronounced axial hypotonia, muscle mass was normal, and muscle strength was MRC 4/5 in arm and leg muscles. In adolescence, her symptoms were stable overall. She is now in a MSc program and has adapted her daily life: she uses an electric bike, she uses the elevator when possible, and prefers typing rather than writing for a long time. Physical examination at the age of 19 showed an elongated face, mild external ophthalmoplegia, mild facial weakness with incomplete forceful eye closure, mild proximal weakness in arms and legs (MRC 4/5), normal muscle mass (Fig.2D, right) and retrognathia (Fig.2D, lower left).

SUPPLEMENTAL FIGURES

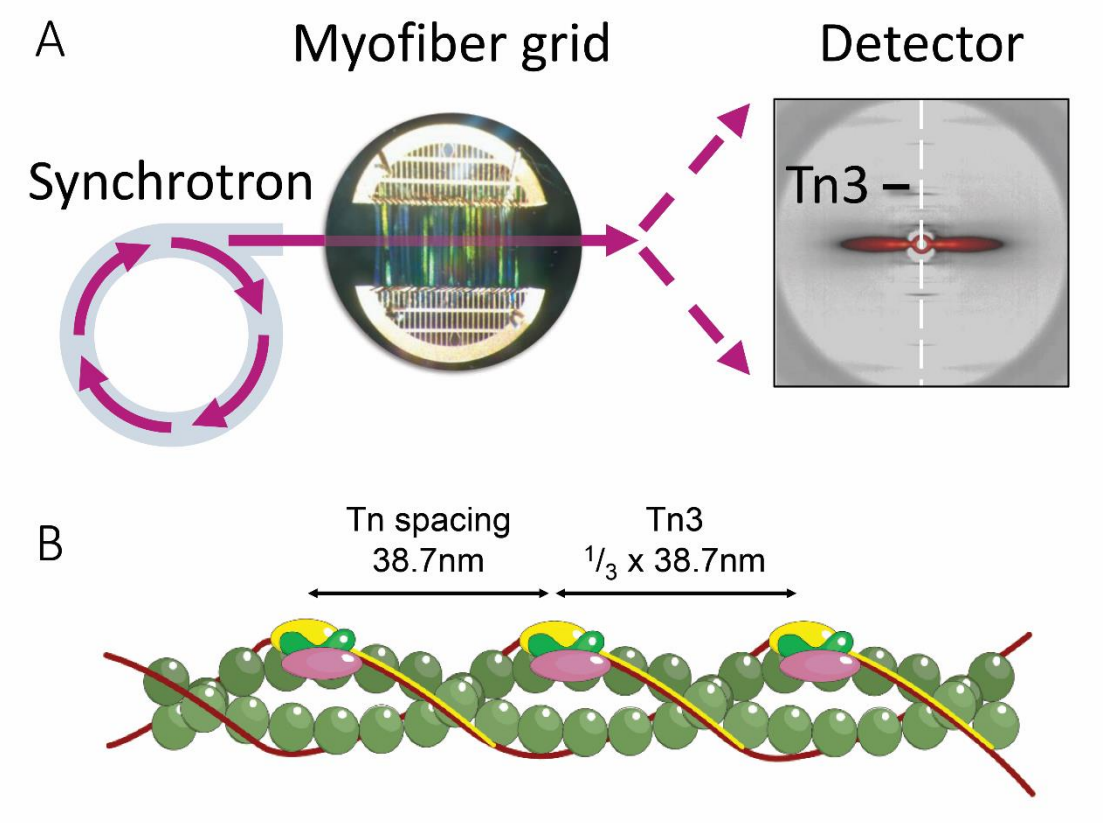

Figure S1. Experimental design of small angle X-ray diffraction experiments. **(A)** Schematic illustrating the X-ray beam, generated by the synchrotron facility at the Advanced Photon Source, and diffracted by 28 myofibers of F1:P1 that are aligned between two halves of an electron microscopy grid. **(B)** schematic of the sarcomeric thin filament showing the spacing between troponin (Tn) complexes and the derivation of the Tn3 reflection.

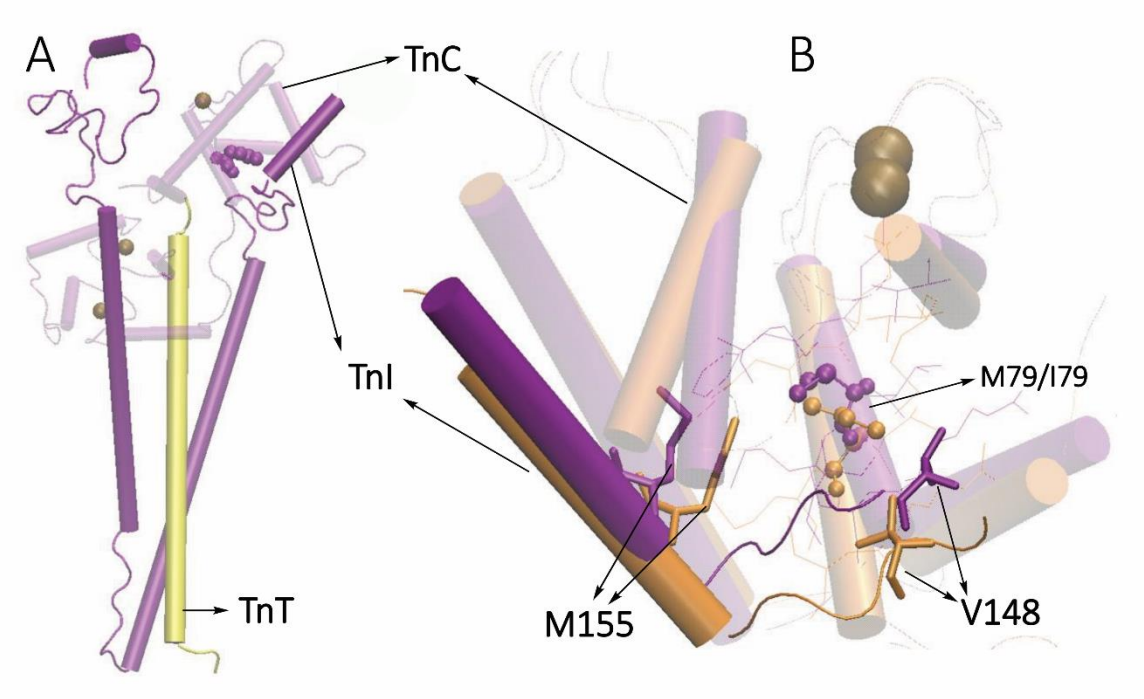

Figure S2. Modeling of WT and M79I variants. **(A)** Crystal structure of cardiac WT TnC, TnI, and TnT complex shown in cartoon representation. TnC is colored purple (transparent), TnI is colored purple (non-transparent) and TnT is colored yellow. Calcium ions are shown as brown spheres. (**B)** N-domain of WT TnC is shown and is colored purple (transparent), whereas the fragment of wild type TnI (spanning residues 145-160) that interacts with TnC's N-domain is shown in purple (non-transparent). Similarly, for the M79I variant these are colored orange. Residues of TnI that interact with the M79/I79 residues are shown as licorice, whereas M79 and I79 of TnC are represented as balls and sticks.

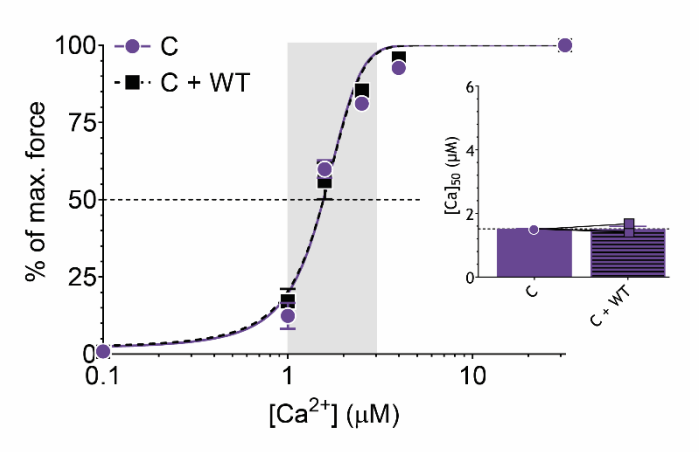

Figure S3. Normalized force-[Ca^{2+}] relation of myofibers from control subjects before and after reconstitution with recombinant WT-fsTnC. Inset shows the [Ca^{2+}] at which 50% of maximum force was reached. The physiological [Ca^{2+}] range is indicated by the gray bar. Data are depicted as mean ± SEM.

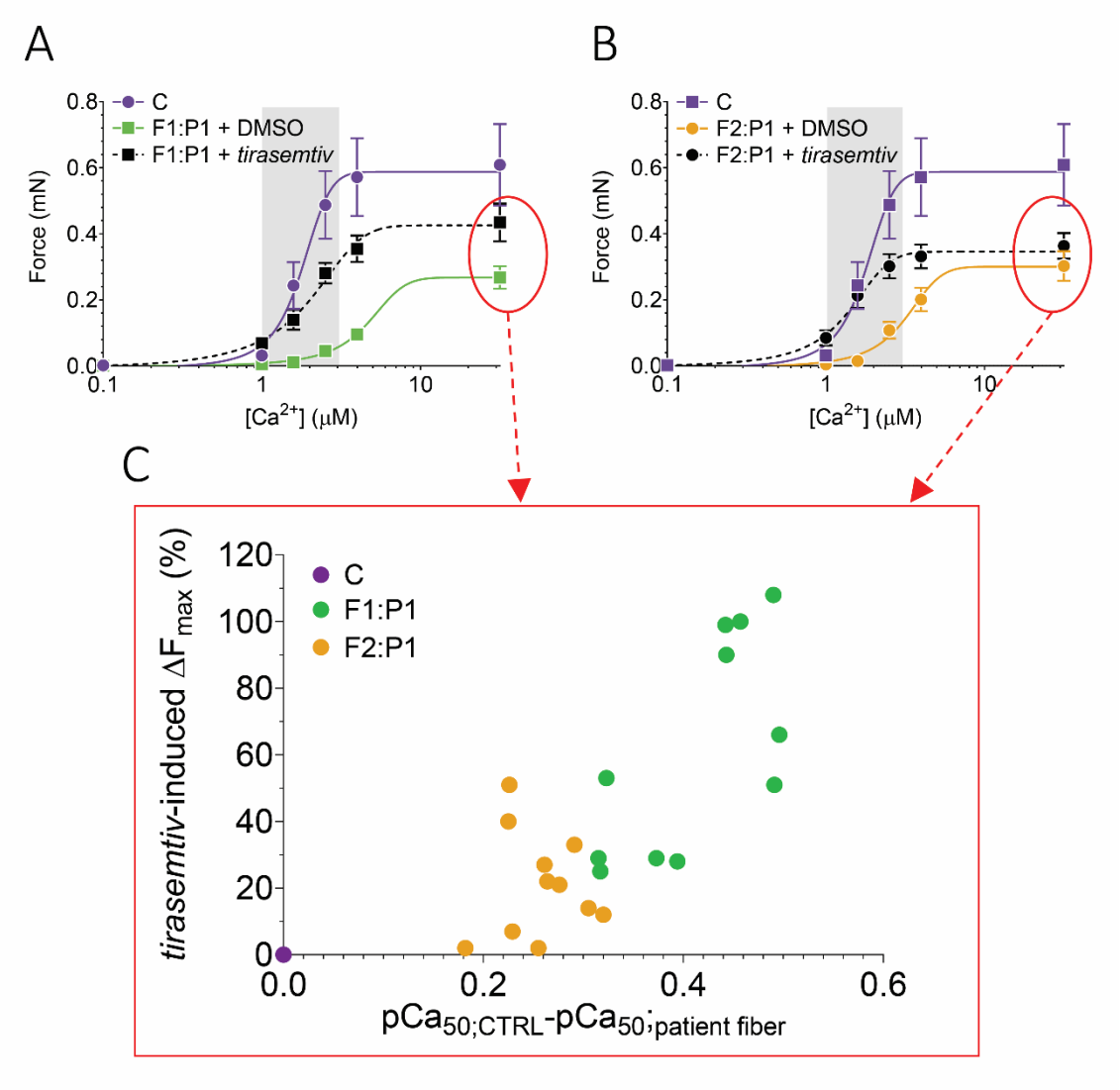

Figure S4. Relation between the *tirasemtiv*-induced increase in maximal force (pCa 4.5) of fast twitch myofibers of patients and the reduced pCa_{50} of these patients' myofibers relative to the pCa_{50} of myofibers of control subjects (C).

SUPPLEMENTAL TABLES

Table S1. Data of fs-TnC reconstitution experiments in control, F1:P1 and F2:P1. Absolute maximal force levels are shown of fast twitch control, F1:P1 and F2:P1 myofibers before the reconstitution protocol (F_0), after endogenous fsTnC extraction (F_E) and after D34Y-/M79I-/WT-fsTnC reconstitution (F_R). Data is depicted as Mean ± SEM.

RECONSTITUTION: force								
Force			Baseline (F_0)	Post-extraction (F_E)		Post-reconstitution (F_R)		
Subject	Protein	(n)	Force (mN)	Force (mN)	% of baseline	Force (mN)	% of baseline	Δ%
Control	WT	3	1.168 ± 0.11	0.448 ± 0.117	37.7 ± 8.6	0.95 ± 0.087	81.7 ± 1.8	44.0
	D34Y	4	1.626 ± 0.086	0.605 ± 0.041	37.5 ± 3.7	0.96 ± 0.071	59.3 ± 2.8	21.8
	M79I	5	1.353 ± 0.119	0.724 ± 0.066	53.6 ± 3.4	0.676 ± 0.059	51 ± 4.1	-2.6
F1:P1	WT/D34Y	6	0.21 ± 0.025	0.032 ± 0.009	14.5 ± 2.5	0.268 ± 0.032	130.7 ± 13.6	116.2
	WT	5	0.303 ± 0.041	0.06 ± 0.016	21.8 ± 1.4	0.325 ± 0.062	113.3 ± 12.6	91.5
F2:P1	WT/M79I	7	0.346 ± 0.024	0.046 ± 0.008	13.4 ± 2.1	0.35 ± 0.025	102.3 ± 5.9	88.9
	WT	6	0.381 ± 0.064	0.111 ± 0.026	27.2 ± 3.5	0.418 ± 0.073	109.3 ± 2.1	82.2

Table S2. Statistical summary of the data shown in Figure 6&S3. A P-value less than 0.05 was considered significant.

RECONSTITUTION: statistical summary					
Force Subject	**Protein**	**(n)**	**Baseline (F_0) [Ca]50**	**Post-reconstitution (F_R) [Ca]50**	***p-value***
Control	WT	3	1.513 ± 0.01	1.508 ± 0.085	0.9518
	D34Y	4	1.763 ± 0.043	3.182 ± 0.079	0.0007
	M79I	5	2.033 ± 0.146	4.822 ± 0.652	0.0007
F1:P1	WT/D34Y	6	4.446 ± 0.318	3.168 ± 0.264	0.0132
	WT	6	3.985 ± 0.527	1.974 ± 0.141	0.0285
F2:P1	WT/M79I	6	2.7 ± 0.27	2.708 ± 0.085	0.9745
	WT	7	3.008 ± 0.222	1.651 ± 0.098	0.0290

Table S3. Statistical summary of the data shown in Figure 7. A P-value less than 0.05 was considered significant.

***TIRASEMTIV*: statistical summary**					
			DMSO	***tirasemtiv***	
Subject	**Fiber type**	**(n)**	**[Ca]50**	**[Ca]50**	***p-value***
F1:P1	Fast	6	5.009 ± 0.332	1.968 ± 0.266	<0.001
F2:P1	Fast	6	3.204 ± 0.139	1.507 ± 0.149	0.0001

REFERENCES

1. Schindelin J, Arganda-Carreras I, Frise E, et al. Fiji: An open-source platform for biological-image analysis. *Nat Methods*. 2012;9(7):676-682. doi:10.1038/nmeth.2019

2. Fischetti R, Stepanov S, Rosenbaum G, et al. The BioCAT undulator beamline 18ID: a facility for biological non-crystalline diffraction and X-ray absorption spectroscopy at the Advanced Photon Source. *J Synchrotron Radiat*. 2004;11(Pt 5):399-405. doi:10.1107/S0909049504016760

3. Wakabayashi K, Sugimoto Y, Tanaka H, Ueno Y, Takezawa Y, Amemiya Y. X-ray diffraction evidence for the extensibility of actin and myosin filaments during muscle contraction. *Biophys J*. 1994;67(6):2422-2435. doi:10.1016/S0006-3495(94)80729-5

4. Houdusse A, Love ML, Dominguez R, Grabarek Z, Cohen C. Structures of four Ca2+-bound troponin C at 2.0 Å resolution: Further insights into the Ca2+-switch int he calmodulin superfamily. *Structure*. 1997;5(12):1695-1711. doi:10.1016/S0969-2126(97)00315-8

5. Romero-Herrera AE, Castillo O, Lehmann H. Human skeletal muscle proteins. The primary structure of troponin C. *J Mol Evol*. 1976;8(3):251-270. doi:10.1007/BF01730999

6. Jo S, Kim T, Iyer VG, Im W. CHARMM-GUI: A web-based graphical user interface for CHARMM. *J Comput Chem*. 2008;29(11):1859-1865. doi:10.1002/jcc.20945

7. Vassylyev DG, Takeda S, Wakatsuki S, Maeda K, Maéda Y. Crystal structure of troponin C in complex with troponin I fragment at 2.3-Å resolution. *Proc Natl Acad Sci U S A*. 1998;95(9):4847-4852. doi:10.1073/pnas.95.9.4847

8. Jorgensen WL, Chandrasekhar J, Madura JD, Impey RW, Klein ML. Comparison of simple potential functions for simulating liquid water. *J Chem Phys*. 1983;79(2):926-935.

doi:10.1063/1.445869

9. Darden TA, Duke RE, Ghoreishi D, et al. AMBER 2018. Published online 2018.

10. Lee J, Cheng X, Swails JM, et al. CHARMM-GUI Input Generator for NAMD, GROMACS, AMBER, OpenMM, and CHARMM/OpenMM Simulations Using the CHARMM36 Additive Force Field. *J Chem Theory Comput*. 2016;12(1):405-413. doi:10.1021/acs.jctc.5b00935

11. Huang J, Rauscher S, Nawrocki G, et al. CHARMM36m: An improved force field for folded and intrinsically disordered proteins. *Nat Methods*. 2016;14(1):71-73. doi:10.1038/nmeth.4067

12. Feller SE, Zhang Y, Pastor RW, Brooks BR. Constant pressure molecular dynamics simulation: The Langevin piston method. *J Chem Phys*. 1995;103(11):4613-4621. doi:10.1063/1.470648

13. Martyna GJ, Tobias DJ, Klein ML. Constant pressure molecular dynamics algorithms. *J Chem Phys*. 1994;101(5):4177-4189. doi:10.1063/1.467468

14. Berendsen HJC, Postma JPM, Van Gunsteren WF, Dinola A, Haak JR. Molecular dynamics with coupling to an external bath. *J Chem Phys*. 1984;81(8):3684-3690. doi:10.1063/1.448118

15. Ryckaert JP, Ciccotti G, Berendsen HJC. Numerical integration of the cartesian equations of motion of a system with constraints: molecular dynamics of n-alkanes. *J Comput Phys*. 1977;23(3):327-341. doi:10.1016/0021-9991(77)90098-5

16. Darden T, York D, Pedersen L. Particle mesh Ewald: An N·log(N) method for Ewald sums in large systems. *J Chem Phys*. 1993;98(12):10089-10092. doi:10.1063/1.464397

17. Roe DR, Cheatham TE. PTRAJ and CPPTRAJ: Software for processing and analysis

of molecular dynamics trajectory data. *J Chem Theory Comput*. 2013;9(7):3084-3095. doi:10.1021/ct400341p

18. Takeda S, Yamashita A, Maeda K, Maeda Y. Structure of the core domain of human cardiac troponin in the Ca(2+)-saturated form. *Nature*. 2003;424(6944):35-41. doi:10.1038/nature01780

19. Rohl CA, Strauss CEM, Misura KMS, Baker D. Protein Structure Prediction Using Rosetta. *Methods Enzymol*. 2004;383:66-93. doi:10.1016/S0076-6879(04)83004-0

20. Humphrey W, Dalke A, Schulten K. VMD: Visual molecular dynamics. *J Mol Graph*. 1996;14(1):33-38. doi:10.1016/0263-7855(96)00018-5

21. van de Locht M, Beecroft SJ, de Winter JM, et al. Recessive MYH7-related myopathy in two families. *Neuromuscul Disord*. 2019;29(6):456-467. doi:10.1016/j.nmd.2019.04.002

22. Joureau B, de Winter JM, Conijn S, et al. Dysfunctional sarcomere contractility contributes to muscle weakness in ACTA1-related nemaline myopathy (NEM3). *Ann Neurol*. 2018;83(2):269-282. doi:10.1002/ana.25144

23. Winter JM de, Joureau B, Lee E-JJ, et al. Mutation-specific effects on thin filament length in thin filament myopathy. *Ann Neurol*. 2016;79(6):959-969. doi:10.1002/ana.24654

24. Ottenheijm CAC, Buck D, de Winter JM, et al. Deleting exon 55 from the nebulin gene induces severe muscle weakness in a mouse model for nemaline myopathy. *Brain*. 2013;136(Pt 6):1718-1731. doi:10.1093/brain/awt113

25. Jasmin BJ, Gardiner PF. Patterns of EMG activity of rat plantaris muscle during swimming and other locomotor activities. *J Appl Physiol*. 1987;63(2):713-718. doi:10.1152/jappl.1987.63.2.713

26. Hooijman PE, Beishuizen A, De Waard MC, et al. Diaphragm fiber strength is reduced in critically Ill patients and restored by a troponin activator. *Am J Respir Crit Care Med*. 2014;189(7):863-865. doi:10.1164/rccm.201312-2260LE

27. Lee E-J, De Winter JM, Buck D, et al. Fast Skeletal Muscle Troponin Activation Increases Force of Mouse Fast Skeletal Muscle and Ameliorates Weakness Due to Nebulin-Deficiency. Ervasti JM, ed. *PLoS One*. 2013;8(2):e55861. doi:10.1371/journal.pone.0055861

28. HILL AV, HILL A, Hill AV. The possible effects of the aggregation of the molecules of haemoglobin on its oxygen dissociation curve. Published online January 1, 1910. Accessed October 9, 2019. https://www.scienceopen.com/document?vid=7a9a2f9a-b092-4ef0-834b-13edd3beae47

29. Walker JS, Li X, Buttrick PM. Analysing force-pCa curves. *J Muscle Res Cell Motil*. 2010;31(1):59-69. doi:10.1007/s10974-010-9208-7

30. Veltri T, De Oliveira GAP, Bienkiewicz EA, et al. Amide hydrogens reveal a temperature-dependent structural transition that enhances site-II Ca 2+ -binding affinity in a C-domain mutant of cardiac troponin C. *Sci Rep*. 2017;7(1). doi:10.1038/s41598-017-00777-6

31. de Winter JM, Buck D, Hidalgo C, et al. Troponin activator augments muscle force in nemaline myopathy patients with nebulin mutations. *J Med Genet*. 2013;50(6):383-392. doi:10.1136/jmedgenet-2012-101470

32. Ottenheijm CA, Witt CC, Stienen GJ, Labeit S, Beggs AH, Granzier H. Thin filament length dysregulation contributes to muscle weakness in nemaline myopathy patients with nebulin deficiency. *Hum Mol Genet*. 2009;18(13):2359-2369. doi:10.1093/hmg/ddp168